



Optimization of subcellular boron distribution measurement using UV-C imprint and neutron autoradiography in boron neutron capture therapy

Yan Wu^a, Diyun Shu^{b,*}, Changran Geng^{a,**}, Ian Postuma^c, Xiaobin Tang^a, Yuan-Hao Liu^{b,a}

^a Department of Nuclear Science and Technology, Nanjing University of Aeronautics and Astronautics, Nanjing, Jiangsu Province, 210016, People's Republic of China

^b Neutron Therapy System Ltd., Xiamen, Fujian Province, 361000, People's Republic of China

^c National Institution of Nuclear Physics, INFN, Unit of Pavia, Pavia, 27100, Italy

ARTICLE INFO

Keywords:

Subcellular boron distribution
Boron neutron capture therapy
Neutron autoradiography
PADC
UV-C imprint

ABSTRACT

The subcellular distribution of boron drugs is crucial for studying radiobiological effects and microdosimetry in boron neutron capture therapy (BNCT). Accurately measuring this distribution remains a key objective. Building on the neutron autoradiography method combined with UV-C sensitization, this study aims to further optimize the approach and implement it at the BNCT center of Xiamen Humanity Hospital, with the expectation of applying it to future boron drug development. A dedicated irradiation device for neutron autoradiography was developed based on a clinical epithermal neutron beam. Optimal conditions for etching and UV-C cell imprints were investigated. After U251 cells were incubated with L-4-boronophenylalanin (BPA), cell imprints and track images were obtained under optimal conditions, and track distributions within cell structure were evaluated. The optimal etching condition involved using Potassium-Ethanol-Water (PEW) solution for 10 min, yielding track diameters of approximately 1 μm . After the poly allyl diglycol carbonate (PADC) with cultured cells was exposed to UV-C for 12 h, a clear cellular structure was imprinted on the PADC. The coupled track and cell structure images suggest that BPA may concentrate more around the U251 cell nucleus. The results demonstrate that the improved method can clearly distinguish tracks within the nucleus and cytoplasm in two-dimensional projections, enabling a more accurate evaluation of boron distribution at the subcellular scale.

1. Introduction

Boron neutron capture therapy (BNCT) is a cancer treatment modality that operates as a binary targeted therapy, relying on a combination of a boron drug and a neutron beam (Barth et al., 2018). The underlying mechanism involves the capture of thermal neutrons by the ^{10}B isotope, which produces Li-7 and an alpha particle. These ionizing particles possess high linear energy transfer (LET) with a tissue penetration range comparable to the size of a single cell, enabling the selective destruction of cancer cells while sparing surrounding normal tissue (Moss, 2014). Because of this biological targeting, the subcellular distribution of boron drugs can significantly influence the radiobiological effects. Therefore, assessing the subcellular distribution of boron drugs is crucial for understanding these effects and for the development of new boron drugs in BNCT (Sato et al., 2018; Sauerwein et al., 2021).

Over an extended period, neutron autoradiography has been employed extensively to measure boron concentration in BNCT, owing

to its sensitivity to the secondary particles produced by the boron neutron capture reaction. Numerous researchers have utilized this method to quantify boron concentration in innovative boron drugs within tissue and cell samples (Bortolussi et al., 2014). It has also been applied to evaluate boron distribution in tissue samples, facilitating the determination of the non-uniform distribution of boron drugs (Wittig et al., 2008). This technique utilizes solid-state nuclear track detectors (SSNTD) to capture the tracks of heavy charged particles. When high LET α or Li-7 particles penetrate the SSNTD, they cause microscopic damage known as latent tracks. After these tracks are etched in a specific chemical solution, they become visible under an optical microscope, with each track corresponding to a single boron neutron capture reaction (Schollmeier et al., 2023). The underlying principle of this method suggests its potential application in measuring boron distribution at the subcellular scale.

Many attempts have been made to utilize neutron autoradiography to obtain the subcellular boron distribution. Ian Postuma et al., 2021

* Corresponding author.

** Corresponding author.

E-mail addresses: shudiyun@neutron.com (D. Shu), gengchr@nuaa.edu.cn (C. Geng).

created reference points on PADC to relocate cell positions precisely, enabling the coupling of track images with cell structure images at the same locations. Satoshi Takeno et al. (2021) conducted a study with the same purpose, but they used ink marks as reference points. In addition to this method, Agustina Portu et al. (2015, 2016) have proposed the use of ultraviolet imprints to achieve simultaneous imaging of tracks and cell structures, avoiding positional deviations during the coupling process of the two images. To achieve optimal results, they studied the impact of different conditions on the quality of the cell imprints. The essence of these methods is to display tracks within the cell structure image clearly and accurately. However, this goal has not yet been fully realized, and further improvements are needed in terms of accuracy, resolution, and the ability to obtain three-dimensional distribution.

Building on the method of simultaneous imaging of cell structures and tracks through UV-C imprints, this work aims to optimize and implement this technique further at the Xiamen Humanity Hospital BNCT Center, with the goal of obtaining boron distribution more accurately at the subcellular scale. The previous method involved the imprints of cell structures on the PADC. In contrast, the optimized method uses imprints of cell structure as a reference to align the track image with a stained cell structure image, making it easier to distinguish the tracks within the cell nucleus and cytoplasm clearly.

2. Materials and methods

2.1. Procedure of subcellular boron distribution measurement

In this study, the poly allyl diglycol carbonate (PADC), also known as CR-39, was utilized as the SSNTD for neutron autoradiography. PADC is a highly efficient particle detector with a linear energy transfer (LET) threshold of $3.5 \text{ keV } \mu\text{m}^{-1}$ (in water), allowing it to detect heavy ions and recoil protons while remaining insensitive to gamma rays and electrons (Ogawara et al., 2020). This characteristic is crucial for accurately measuring the distribution of boron drugs, as it effectively minimizes interference from other factors. Nonetheless, it is also necessary to consider the impact of proton tracks on these measurements. The exclusion of proton tracks can be achieved by optimizing the etching conditions, a topic that will be elaborated upon later.

The modified steps of the optimized method will be detailed in Section 2.6. Briefly, imaging the imprints of cell structures and tracks at the same location is achieved by adjusting the focal plane. Then the imprints of the cell structure images serve as a reference for accurately coupling the track image with the stained cell structure image. Each step of the flowchart will be described in more detail in the following

sections.

2.2. Preparation of cell samples

In this study, glioblastoma U251 MG cells, purchased from Pricella Biotechnology, were used. The cells were seeded in 10-cm culture dishes containing high-glucose Dulbecco's Modified Eagle Medium (DMEM) supplemented with 10% fetal bovine serum (Gibco; Thermo Fisher Scientific, Austin, TX) and 1% penicillin-streptomycin (Invitrogen; Thermo Fisher Scientific, Austin, TX). A sterile PADC ($7.5 \times 2.5 \text{ cm}$) was also placed in each culture dish. In Step 1 of Fig. 1, the cells were cultured at 37°C with 5% CO_2 for 12 h. As shown in Step 2, the medium was replaced with DMEM containing 50 ppm BPA (NBB-001, Neuboron Bio-SciTech, Xiamen, Fujian, China) and the cells were incubated under the same conditions for an additional 3 h. After boron drug incubation, the PADC was removed and washed five times with phosphate buffered solution (PBS). The cells were then fixed with 4% paraformaldehyde to prevent boron migration and to secure them onto the PADC, as outlined in Step 3 in Fig. 1. For samples requiring cell staining, hematoxylin and eosin staining was performed after cell fixation. Partial efflux of boron may occur during staining and fixation; nevertheless, subcellular motion is not a major concern for the actual application of the proposed technique (Portu et al., 2015).

2.3. Irradiation device development

Neutron autoradiography relies on boron neutron capture reactions, where a high thermal neutron flux is advantageous for enhancing measurement efficiency. The NeuPex accelerator-based boron neutron capture therapy (AB-BNCT) system, installed at the BNCT center of Xiamen Humanity Hospital provides a clinical-grade epithermal neutron beam (Wang et al., 2024). This epithermal neutron beam is not suitable for neutron autoradiography, so it is necessary to design an irradiation device to moderate the neutrons and accommodate the samples. This device is installed in the moderator cavity of the beam shaping assembly during irradiation. The structure of the device is shown in Fig. 2. It is divided into two layers: the neutron moderation layer and the neutron reflection layer. Sample cavities are set on the inner side of the neutron moderation layer, allowing the placement of liquid, tissue, and cell samples. PE (polyethylene) and PMMA (polymethyl methacrylate) were selected as materials for the device. The thermal neutron flux at the sample location under different material and thickness conditions was studied using the PHITS Monte Carlo code (Version 3.28) to determine the optimal design. The neutron irradiation time for cell experiments in

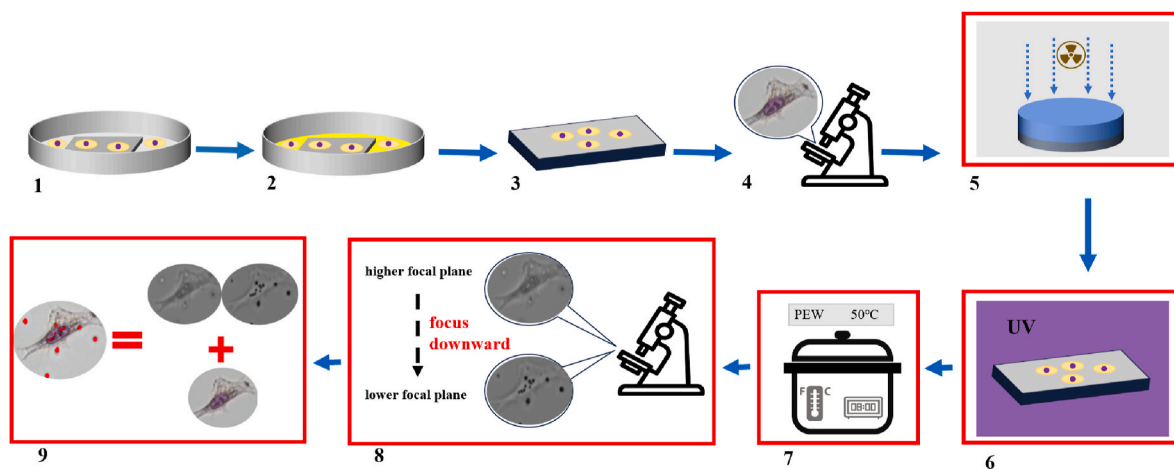


Fig. 1. Flow chart of subcellular boron distribution measurement method. (1) Incubate cells on PADC; (2) co-incubate with the boron drug; (3) fix and stain cells; (4) acquire image of cells; (5) perform neutron irradiation with the device; (6) exposure sample to UV-C light; (7) remove cells from PADC and etch; (8) acquire cell imprints and tracks images; (9) couple images for analysis.

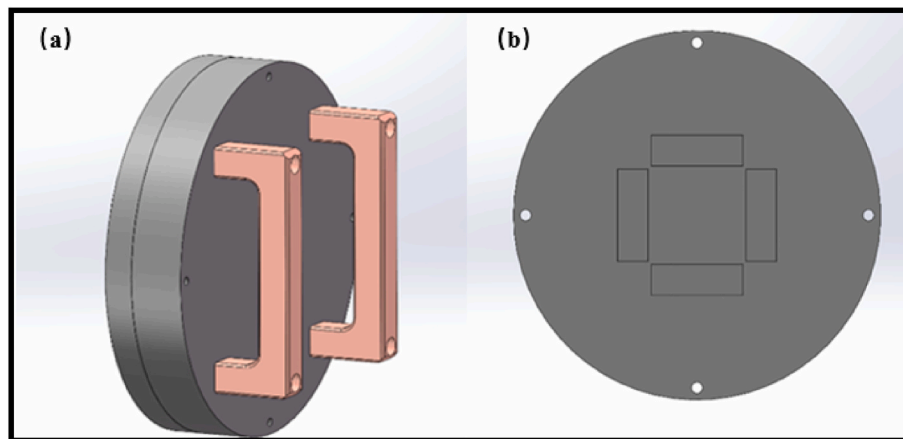


Fig. 2. Structure design of the irradiation device. (a) Overall design of the irradiation device; (b) design of moderation layer with sample cavities.

this study will be determined based on the design results.

To ensure the comparability of boron concentration measurements in samples using different cavities, it is crucial to verify the consistency of neutron irradiation conditions. Three experimental rounds were conducted using boric acid solutions at different concentrations. In each round, solutions with identical concentrations were placed in four sample cavities and then irradiated for 1 min. Subsequently, the track density on PADC was examined under identical etching conditions across various sample cavities within the same experiment.

2.4. Cell imprints with UV-C exposure

As depicted in Step 6 of Fig. 1, the formation of cell imprints on PADC requires exposure to ultraviolet C (UV-C) light. UV irradiation transfers energy to PADC, causing excitation and ionization of molecular chains, which result in radical formation, scission of the main chain bonds, and crosslinking of polymer chains. These chemical alterations degrade the physical, mechanical, and optical properties of the polymers, consequently influencing both the bulk and track etching responses (de Vasconcelos et al., 2019; Kusumoto et al., 2019). When PADC with cultured cells is exposed to UV-C light, the regions beneath the cells exhibit varying degrees of damage compared with the surrounding areas due to the cells' absorption of UV-C light. Additionally, there are differences in UV-C absorption between the cell nucleus and the cytoplasm. By utilizing these variations in UV-C induced damage on PADC, it becomes possible to imprint the cell structure onto the PADC after etching. In this study, UV-C light with a wavelength of 254 nm was used for cell imprints, and the optimal conditions were investigated. Ten stained samples were exposed to UV-C light for durations ranging from 3 to 30 h, with 3-h intervals. Similarly, 10 unstained samples were exposed to UV-C light under the same conditions to assess the effects of staining on cell imprints. All samples were irradiated at a distance of 3 cm from the UV-C lamp.

2.5. Chemical etching of PADC

As shown in Step 7 of Fig. 1, the formation of visible tracks and cell imprints requires chemical etching of PADC. During neutron irradiation of the sample, in addition to the desired α and Li-7 particles, protons are generated, which can create tracks on the PADC. It is preferable that the tracks generated by protons be eliminated during the etching process. Furthermore, to achieve high-resolution measurement of subcellular boron distribution, it is essential that the tracks remain sufficiently small. Therefore, the chemical etching conditions need to be optimized.

Based on the above considerations, the PEW solution, composed of ethanol, potassium hydroxide, and pure water, was selected as the chemical etching solution. To investigate the impact of alcohol mass

fraction on the removal of proton tracks, deionized water was utilized as the sample. Deionized water was selected due to its composition of only hydrogen and oxygen, which under neutron irradiation would produce only proton tracks. After neutron irradiation for 1 min, PEW solutions with varying alcohol mass fractions were employed for etching to determine the presence of proton tracks. The alcohol mass fraction in the PEW solutions was set to 5, 15, 25, 30%, 35, and 40%. During the etching process, the bath temperature was maintained at 50 °C, as higher temperatures have been shown to potentially damage PADC (Ogawara et al., 2020). To control track size and ensure alignment with subcellular scale distribution measurements, a boric acid solution containing 25 ppm ^{10}B was used. Following neutron irradiation for 3 min, the optimal etching solution was applied for durations of 10, 20, 30, and 40 min to analyze track sizes.

2.6. Image acquisition and coupling

In this study, images of cell structures, cell imprints, and tracks were obtained using a Keyence BZ-800X all-in-one fluorescence microscope in bright-field imaging mode at 40 \times or 60 \times magnifications. In Step 4 of Fig. 1, cell structure images were captured using a 40 \times objective, and the coordinates of each image were recorded for relocation in Step 8. In Step 8, the focal plane was first adjusted to capture the cell imprints image and then moved downward to capture the track image. Both images were taken at the same location.

The cell imprints image provides a clear outline of the cell, which allows precise alignment of the cell structure image with the cell imprints. Based on this alignment, the necessary rotation and offset for the cell structure image can be determined. Since the cell imprints and track images are captured from the same position, the same rotation and offset can then be applied to align the cell structure image with the track image. This results in an accurate track distribution based on the cell structure image. All image alignment processes were carried out using Python (Version 3.12.5).

3. Results and discussion

3.1. Irradiation device and its validation

As shown in the left panel of Fig. 3, PE demonstrates superior moderating effectiveness compared with PMMA, likely due to its higher hydrogen content. Consequently, PE was chosen as the material for the irradiation device, and further investigations were conducted at various thicknesses. As the thickness of PE increases, the peak thermal neutron flux initially increases gradually, but the rate of increase subsequently slows down (as shown in the right panel of Fig. 3). When the thickness increases from 7 cm to 8 cm, the epithermal neutron flux at the peak

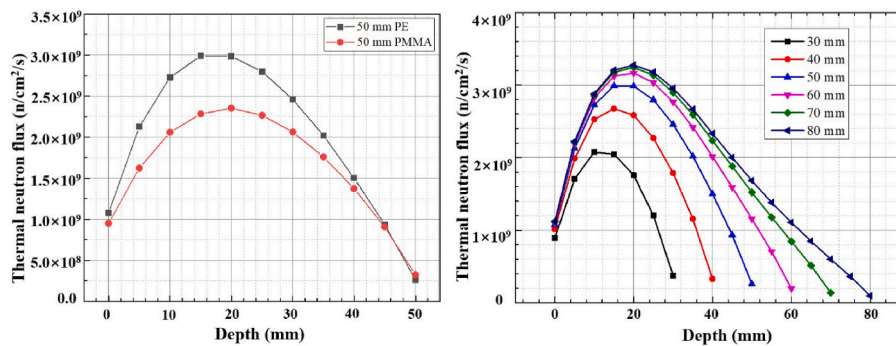


Fig. 3. Thermal neutron flux distribution at different depths with 5-cm-thick PE and PMMA (left panel) and with varying PE thicknesses (right panel).

shows only a slight increase. To achieve the maximum thermal neutron flux, a PE thickness of 8 cm was selected, with the sample cavities positioned at 2 cm. The irradiation device was thus designed to include a 2-cm PE layer as the moderator and a 6-cm PE layer as the reflector. In this configuration, the theoretical thermal neutron flux at the sample position reaches $3.25 \times 10^9 \text{ n cm}^{-2} \text{ s}^{-1}$. Under these conditions, the irradiation time is set to 25 min for neutron autoradiography of cell samples.

As shown in Fig. 2, multiple sample cavities were arranged within the inner moderator layer. The track densities on PADC at the four sample cavities under boric acid solution with the identical concentration are presented in Table 1. The track densities on PADC at different sample positions in each experiment were almost identical, with Relative Standard Deviation (RSD) all below 2%, indicating that the four sample positions can be considered to have received nearly identical neutron beam irradiation.

3.2. Determination of the etching conditions

The result of PADC etched by PEW solutions with various ethanol mass fractions are shown in Fig. 4. Proton tracks are still observable when the alcohol concentration in the PEW solution is below 35%. However, with alcohol concentrations of 35% and 40% in the PEW solution, no proton tracks were observed within the field of view. PEW with 35% alcohol concentration (PEW35) was ultimately chosen as the etching solution.

Fig. 5 shows track images obtained from PADC etched with PEW35 for various durations. When the etching time is 10 min, the average track diameter is approximately $1 \mu\text{m}$. As the etching time increases to 40 min, the average track diameter grows to over $2 \mu\text{m}$. Considering that a $1\text{-}\mu\text{m}$ track diameter is more suitable for subcellular track distribution measurements relative to a cell diameter of $10 \mu\text{m}$, an etching time of 10 min is selected.

3.3. Determination of the UV-C exposure conditions

For cells cultured on PADC, the quality of cell imprints was investigated under both stained and unstained conditions Fig. 6 shows the cell imprint images of unstained cell samples after different durations of UV-C exposure. When the UV-C exposure time was increased to 21 h, the cell imprint images could distinguish between the cell nucleus and

cytoplasm. For stained cell samples, after just 3 h of UV-C exposure, the cell imprint images could already distinguish between the cell nucleus and cytoplasm (as shown in Fig. 7). This may be because the stain enhances the absorption of UV-C light within the cell region. Specifically, the cell nucleus and cytoplasm absorb the stain to different extents, resulting in higher contrast in their imprints, making them more distinguishable. To further improve the distinction between the cell nucleus and cytoplasm in subcellular boron distribution measurements, we chose to stain the cell samples and then expose them to UV-C light for 12 h.

3.4. Distribution of BPA in U251 cells

Based on the optimized cell imprints and etching conditions, the subcellular distribution of BPA within U251 cells was measured using the improved method. Fig. 8a shows the stained cell structure image in a specific field of view, while Fig. 8b and c represent the cell imprint image and the track image, respectively. Using the method introduced in Section 2.6, the above three images can be coupled to obtain a precise track distribution map based on the cellular structure image (Fig. 8d).

From the results shown in the figure, a small number of tracks can still be observed outside the cells. These tracks are likely due to residual boron drugs that were not completely removed and remained adhering to the surface of the PADC. Because these residues are closely attached to the PADC surface, the secondary particles generated from reactions with thermal neutrons penetrate the PADC directly without significant energy loss. As a result, these secondary particles have higher energy and greater penetration depth, leading to a significantly larger size of the tracks than of those within the cell projection areas. On one hand, these tracks are located outside the cell boundaries; on the other, their larger size allows them to be distinguished easily. Therefore, the presence of these tracks does not impact the analysis of the measurement results.

In Fig. 8, the tracks appear almost circular, indicating that the particles are nearly vertically incident on the PADC. This pattern reflects the distribution of reaction sites within cells, particularly the distribution of boron drugs. In reality, the particles produced by the neutron capture reaction are isotropic in direction. Some particles stop directly within the cells, while others, due to their angle of incidence, have a shorter traversal distance in the vertical direction and do not reach the etching depth (Yasuda et al., 2008). Consequently, most tracks observed at the etching depth of the PADC are from nearly vertically incident charged particles.

If charged particles are generated near the cell boundaries in proximity to the PADC detector, they may penetrate to the etching depth despite striking the PADC at an inclination. Consequently, tracks generated by charged particles incident at an angle may also appear on the PADC. To further analyze the track formation, a $60\times$ magnification was used for detailed observation and analysis. As shown in Fig. 9, the morphology of the tracks becomes clearer under $60\times$ magnification, with tracks incident from different directions displaying distinct shapes.

Table 1

The track densities on PADC at different sample positions under the same boron concentration.

	Position 1 (/mm ⁻²)	Position 2 (/mm ⁻²)	Position 3 (/mm ⁻²)	Position 4 (/mm ⁻²)	RSD
Trial 1	1957	1894	1921	1936	1%
Trial 2	5913	5954	6073	5865	2%
Trial 3	5842	5948	6057	6022	2%

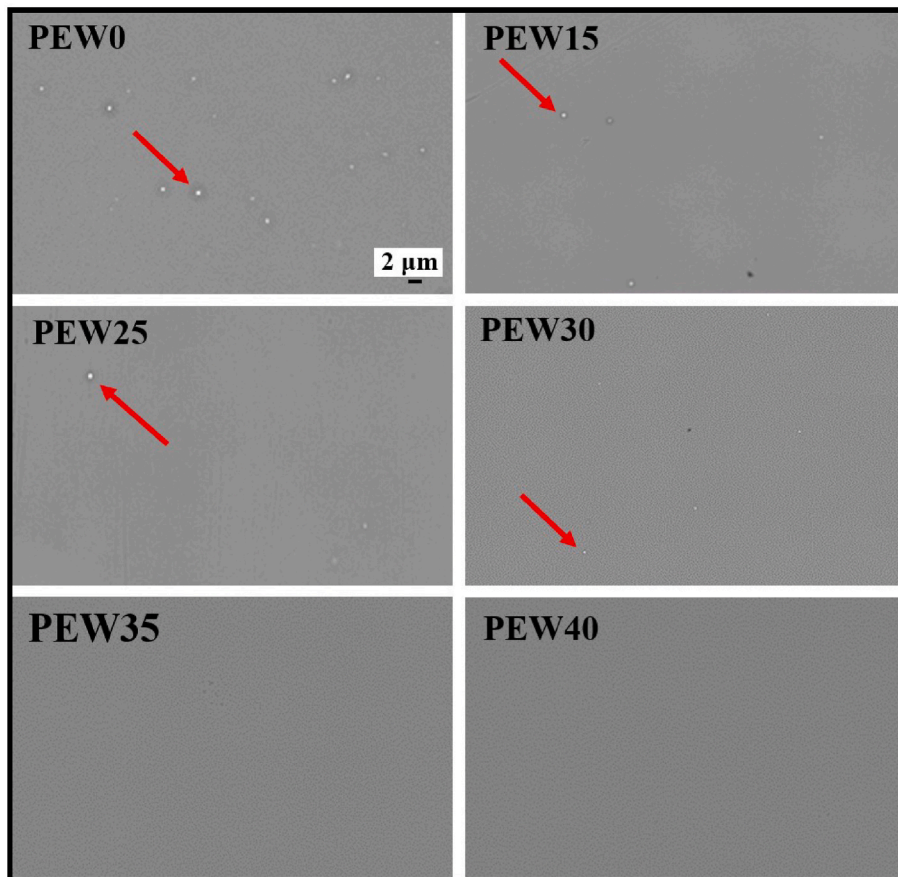


Fig. 4. The track images of the PADC etched with PEW solutions with different alcohol mass fractions after deionized water sample irradiation.

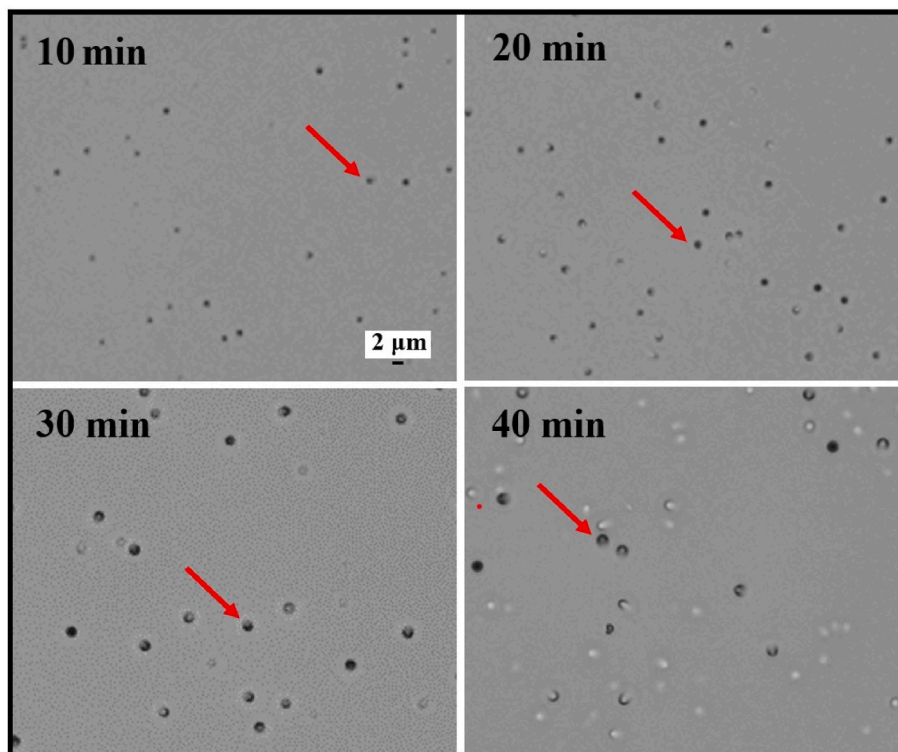


Fig. 5. Track images obtained from PADC etched with PEW35 for various durations after 25 ppm ¹⁰B of boric acid solution irradiation: (a) 10 min; (b) 20 min; (c) 30 min; (d) 40 min.

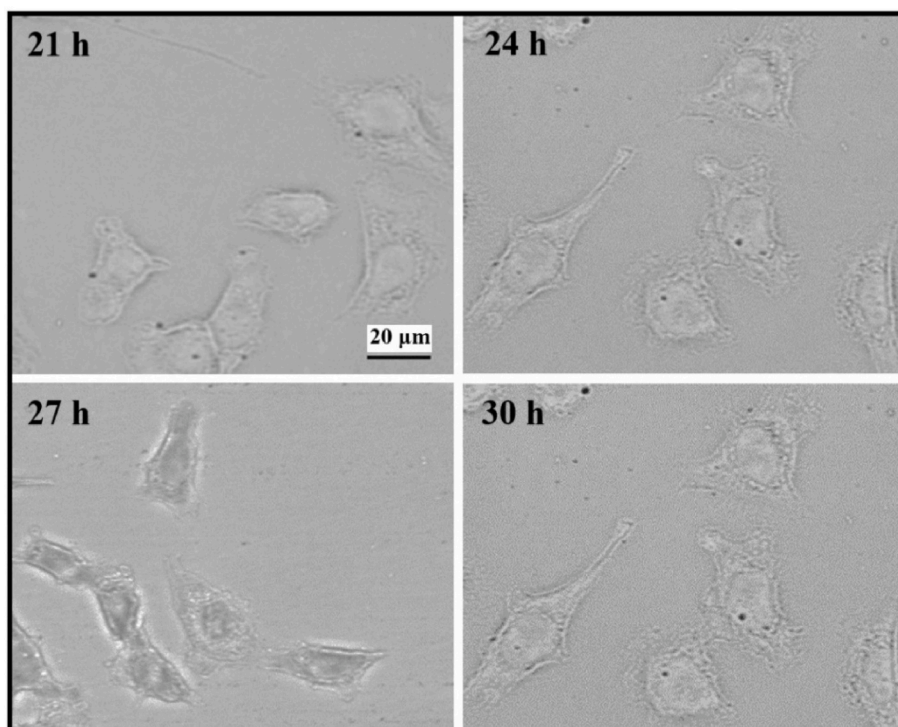


Fig. 6. Cell imprint images of unstained cell samples after different durations of UV-C exposure.

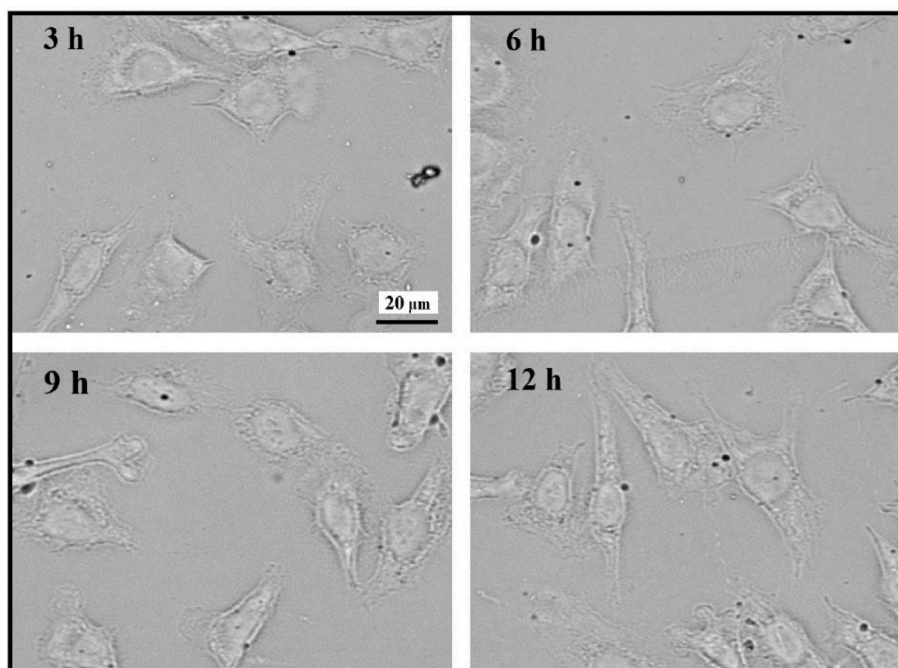


Fig. 7. Cell imprint images of stained cell samples after different durations of UV-C exposure.

For instance, comet-like tracks suggest an oblique incidence into the PADC, with the tail of the comet indicating the direction of particle entry (Al-Khalil et al., 2022; Sato et al., 2008). By analyzing these track characteristics, a more accurate distribution of tracks within the cell can be inferred. For example, the track indicated by the arrow in Fig. 9, if judged solely by its position relative to the cell imprint, might incorrectly be assumed to originate from ^{10}B within the cell. In reality, however, this track is caused by ^{10}B located outside the cell.

To enhance the reliability of subcellular track distribution measurements, the aforementioned methods were employed to exclude invalid tracks, and the distribution of tracks in 200 cells was analyzed and statistically evaluated, as shown in Table 2. The results indicated that the tracks were predominantly concentrated in the projected area of the cell nucleus. However, it is widely recognized that BPA does not easily penetrate the cell nucleus (Chandra and Lorey, 2007; Braun et al., 2003). Therefore, it can be inferred that BPA is most likely concentrated

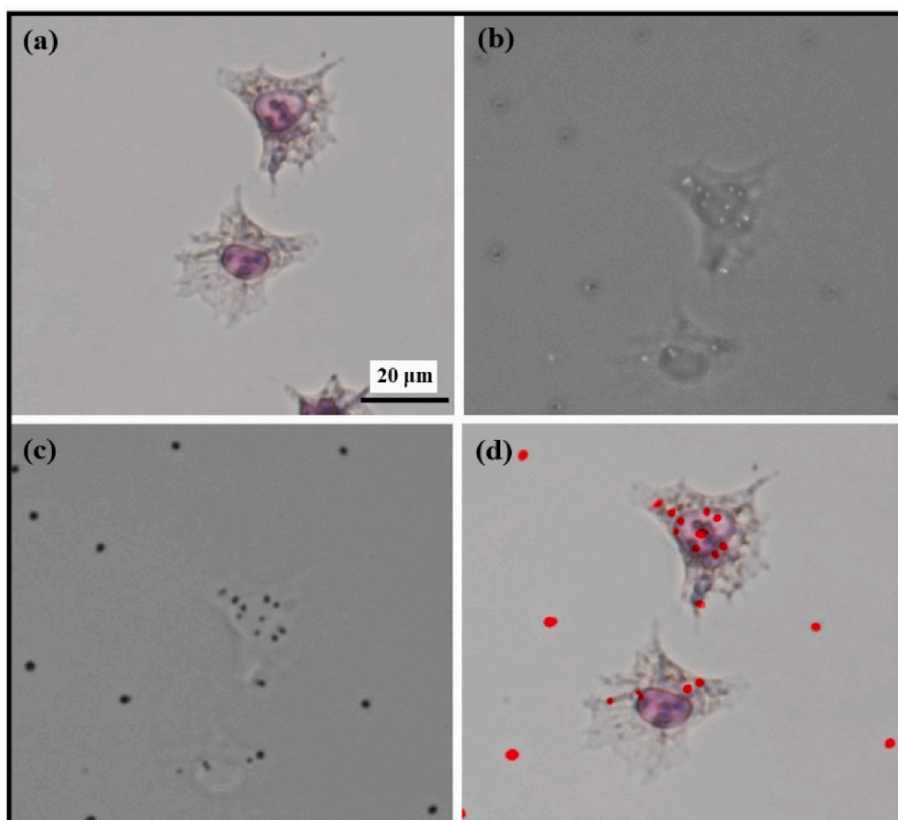


Fig. 8. (a) Cell imprints image; (b) track image; (c) stained cell images; (d) accurate coupled image of tracks and cells.

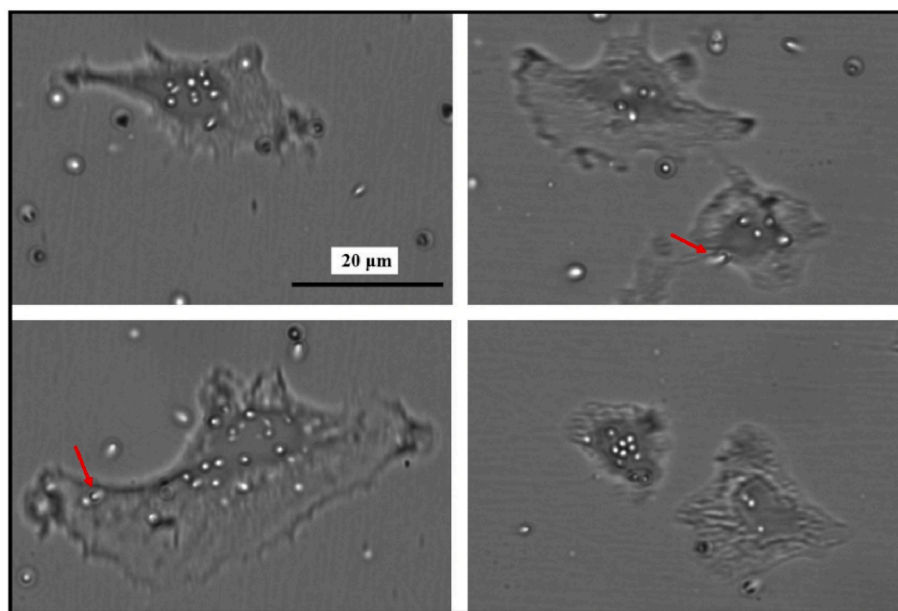


Fig. 9. The cell imprints images under 60 × magnification, simultaneously showing the morphology of the tracks.

Table 2

The average number of tracks at the subcellular scale and their corresponding proportions based on the statistical results of 200 cells.

	Nucleus/Membrane	Cytoplasm	Cytomembrane
Average number of tracks	8	3	1
Average proportion	67%	25%	8%

on the nuclear membrane or near to the nucleus in U251 cells, which would explain the observed concentration of tracks in the nuclear projection area in the two-dimensional view. Nevertheless, it is important to note that the nucleus is not a simple spherical structure, so this conclusion cannot be made with absolute certainty.

Meanwhile, it is important to emphasize that BPA uptake by cells varies across different phases of the cell cycle (Matsuya et al., 2024). In

this study, identifying cells accurately at specific stages of the cell cycle based on the available images was challenging; therefore, the effect of the cell cycle on boron uptake was not included in the analysis. However, cells at various stages can be effectively distinguished using specific histological staining methods or, alternatively, cell synchronization techniques can be employed to arrest cells at a uniform phase. These strategies would facilitate a systematic investigation into the differential boron uptake across cell cycle phases, which will be prioritized in future research.

4. Conclusions

This work details the successful implementation of an enhanced neutron autoradiography method at the BNCT Center of Xiamen Humanity Hospital. The design of the irradiation device was tailored to improve measurement efficiency by increasing the thermal neutron flux. Optimization of etching conditions enabled the acquisition of appropriate-sized tracks for subcellular measurements while excluding proton tracks. Additionally, optimization of UV-C exposure conditions allowed clear imprints of cellular contours and structures on PADC. Moreover, the clear cellular structures reflected by high-quality cell imprints not only allow us to couple track images with cell images but also enable further assessment of track origins by analyzing their morphology. This facilitates high-quality subcellular-scale measurements of boron drugs.

This work will provide effective support for evaluating the efficacy of boron drugs by offering more accurate measurements of their subcellular distribution. However, the method still has limitations, as the accurate three-dimensional distribution of boron drugs within cells remains unattainable. In future work, we can consider using machine learning to further process the two-dimensional morphology of tracks and accurately infer the spatial positions of the particles that produced the tracks (Amit et al., 2022; Kaur and Dhir, 2024; Yoshida et al., 2021; Akselrod et al., 2020).

CRedit authorship contribution statement

Yan Wu: Writing – original draft, Software, Methodology, Investigation, Formal analysis, Data curation, Conceptualization. **Diyun Shu:** Writing – review & editing. **Changran Geng:** Writing – review & editing. **Ian Postuma:** Writing – review & editing. **Xiaobin Tang:** Writing – review & editing. **Yuan-Hao Liu:** Writing – review & editing.

Declaration of competing interest

The authors declare that they have no known competing financial interests or personal relationships that could have appeared to influence the work reported in this paper.

Acknowledgments

This work is supported by the National Key Research and Development Program of China (Grant 2022YFE0107800, Grant 2023YFE0197700); the National Natural Science Foundation of China (Grant 12261131621); and the Natural Science Foundation of Jiangsu Province (Grant BK20220132).

Data availability

Data will be made available on request.

References

- Akselrod, M., Fomenko, V., Harrison, J., 2020. Latest advances in FNTD technology and instrumentation. *Radiat. Meas.* 133, 106302.
- Al-Khalil, Y.T., et al., 2022. On the question of track etch rate amplitude variation in the Bragg-peak vicinity: experimental verification for low-energy α -particle tracks in CR-39. *Nucl. Instrum. Methods Phys. Res. Sect. A Accel. Spectrom. Detect. Assoc. Equip.* 1031.
- Amit, G., Mosseri, I., Even-Hen, O., Schneider, N., Fisher, E., Datz, H., Cohen, E., Nissim, N., Batani, D., 2022. Particles detection system with CR-39 based on deep learning. *Laser Part. Beams* 2022, e12.
- Barth, R.F., Zhang, Z., Liu, T., 2018. A realistic appraisal of boron neutron capture therapy as a cancer treatment modality. *Cancer Commun.* 38, 36.
- Bortolussi, S., et al., 2014. Boron concentration measurements by alpha spectrometry and quantitative neutron autoradiography in cells and tissues treated with different boronated formulations and administration protocols. *Appl. Radiat. Isot.* 88, 78–80.
- Braun, K., et al., 2003. The enhancement of neutron irradiation of HeLa-S cervix carcinoma cells by cell-nucleus-addressed deca-p-boronophenylalanine. *Eur. J. Med. Chem.* 38, 587–595.
- Chandra, S., Lorey, D.R., 2007. SIMS ion microscopy imaging of boronophenylalanine (BPA) and $^{13}\text{C}^{15}\text{N}$ -labeled phenylalanine in human glioblastoma cells: relevance of subcellular scale observations to BPA-mediated boron neutron capture therapy of cancer. *Int. J. Mass Spectrom.* 260, 90–101.
- de Vasconcelos, D.A., Ciolini, R., d'Errico, F., 2019. A new sensitization technique combining CO₂ and UV treatments for improved neutron dosimetry of CR-39 track detectors. *Radiat. Meas.* 125, 85–88.
- Kaur, K., Dhir, R., 2024. Deep learning based hybrid ghost-net for metaspread chromosome image segmentation. *Biomed. Signal Process Control* 95, 106298.
- Kusumoto, T., Mori, Y., Kanasaki, M., Oda, K., Kodaira, S., Barillon, R., Yamauchi, T., 2019. Drastic decrease of carbonyl group after the loss of ether in PADC exposed to 222 nm UV photons. *Radiat. Phys. Chem.* 157, 60–64.
- Matsuya, Y., Sato, T., Kusumoto, T., Yachi, Y., Seino, R., Miwa, M., Ishikawa, M., Matsuyama, S., Fukunaga, H., 2024. Cell-cycle dependence on the biological effects of boron neutron capture therapy and its modification by polyvinyl alcohol. *Sci. Rep.* 14 (1), 16696.
- Moss, R.L., 2014. Critical review, with an optimistic outlook, on boron neutron capture therapy (BNCT). *Appl. Radiat. Isot.* 88, 2–11.
- Ogawara, R., Kusumoto, T., Konishi, T., Hamano, T., Kodaira, S., 2020. Detection of alpha and ^7Li particles from ^{10}B (n, α) ^7Li reactions using a combination of CR-39 nuclear track detector and potassium hydroxide-ethanol-water solution in accelerator-based neutron fields. *Nucl. Instrum. Methods Phys. Res. Sect. B Beam Interact. Mater. Atoms* 467, 9–12.
- Portu, A., et al., 2015. Simultaneous observation of cells and nuclear tracks from the boron neutron capture reaction by UV-C sensitization of polycarbonate. *Microsc. Microanal.* 21, 796–804.
- Portu, A.M., et al., 2016. Experimental set up for the irradiation of biological samples and nuclear track detectors with UV C. *Rep. Practical Oncol. Radiother.* 21, 129–134.
- Postuma, I., et al., 2021. Colocalization of tracks from boron neutron capture reactions and images of isolated cells. *Appl. Radiat. Isot.* 167, 109353.
- Sato, F., Kuchimaru, T., Kato, Y., Iida, T., 2008. Digital image analysis of etch pit formation in CR-39 track detector. *Jpn. J. Appl. Phys.* 47.
- Sato, T., Masunaga, S.I., Kumada, H., Hamada, N., 2018. Microdosimetric modeling of biological effectiveness for boron neutron capture therapy considering intra- and intercellular heterogeneity in ^{10}B distribution. *Sci. Rep.* 8, 988.
- Sauerwein, W.A.G., et al., 2021. Theranostics in boron neutron capture therapy. *Life* 11.
- Schollmeier, M.S., et al., 2023. Differentiating multi-MeV, multi-ion spectra with CR-39 solid-state nuclear track detectors. *Sci. Rep.* 13, 18155.
- Takeno, S., Tanaka, H., Watanabe, T., Mizowaki, T., Suzuki, M., 2021. Quantitative autoradiography in boron neutron capture therapy considering the particle ranges in the samples. *Phys. Med.* 82, 306–320.
- Wang, X., Shu, D., Geng, C., Tang, X., Liu, Y.H., 2024. Advancing 2D reaction rate measurements in BNCT: validation of the indirect neutron radiography method. *Radiat. Meas.* 174, 107133.
- Wittig, A., et al., 2008. Boron analysis and boron imaging in biological materials for Boron Neutron Capture Therapy (BNCT). *Crit. Rev. Oncol. Hematol.* 68, 66–90.
- Yasuda, N., Zhang, D.H., Kodaira, S., Koguchi, Y., Takebayashi, S., Shinozaki, W., Fujisaki, S., Juto, N., Kobayashi, I., Kurano, M., Shu, D., 2008. Verification of angular dependence for track sensitivity on several types of CR-39. *Radiat. Meas.* 43, S269–S273.
- Yoshida, J., et al., 2021. CNN-based event classification of alpha-decay events in nuclear emulsion. *Nucl. Instrum. Methods Phys. Res. Sect. A Accel. Spectrom. Detect. Assoc. Equip.* 989, 164930.